*Anal. Chem.* **2009,** *81,* 4873–4881

# Optimization of Encoded Hydrogel Particles for Nucleic Acid Quantification

**Daniel C. Pregibon and Patrick S. Doyle***

*Department of Chemical Engineering, Massachusetts Institute of Technology, 77 Massachusetts Avenue, Cambridge, Massachusetts 02139*

**The accurate quantification of nucleic acids is of utmost importance for clinical diagnostics, drug discovery, and basic science research. These applications require the concurrent measurement of multiple targets while demanding high-throughput analysis, high sensitivity, specificity between closely related targets, and a wide dynamic range. In attempt to create a technology that can simultaneously meet these demands, we recently developed a method of multiplexed analysis using encoded hydrogel particles. Here, we demonstrate tuning of hydrogel porosity with semi-interpenetrating networks of poly(ethylene glycol), develop a quantitative model to understand hybridization kinetics, and use the findings from these studies to enhance particle design for nucleic acid detection. With an optimized particle design and efficient fluorescent labeling scheme, we demonstrate subattomole sensitivity and single-nucleotide specificity for small RNA targets.**



Molecular screening lies at the foundation of biological tests in the clinic and at the bench, with specific examples including expression profiling of mRNA to connect drug responses to disease (i.e., the "connectivity map")[1] and microRNA profiling for cancer diagnostics.[2−5] These and most other screening applications require the quantification of tens to thousands of biomarker targets in a single sample. In comparison to serial testing, multiplexed assays require smaller sample volumes, leading to reductions in assay cost and increases in speed. Two broad classes of technologies are used for multiplexing: planar microarrays and particle-based arrays. Although microarrays typically provide superior screening density, particles provide faster kinetics via mixing (although planar kinetics are diffusion-limited), increased capacity afforded by increased surface area, and higher versatility for adapting target sets.[6]

Although particles are preferred over planar substrates for high-throughput screening, current approaches for particle-based multiplexed analysis involve complicated or expensive processes for encoding, functionalizing, or decoding active substrates and also yield a very limited number of analyte-specific codes.[7,8] Few commercial platforms exist and are limited by their coding scheme to scan up to ∼100 targets at a time.[9] This limit in "density" is restrictive for several applications in biomarker discovery, drug discovery, and diagnostics that require the quantification of hundreds or thousands of targets.[1,10] It can also be viewed as a limitation in throughput, when considering sample pooling (simultaneously scanning several samples for few targets). A technology that could accommodate higher density without loss of performance or increase in cost would be an enabling tool.

Beyond limitations in throughput or density, the materials used in most commercial arrays are not ideal for biological interactions. The environment in which ligands are immobilized has tremendous impact on the quality of target capture, dictating how many molecules can bind to a surface, how specific that interaction is for a given molecule, and how strong that binding event is.[11,12] All of these attributes are extremely important for biomolecule quantification as they determine the sensitivity, specificity, and dynamic range of detection. Ideally, substrates used for biomolecule quantification would be based on nonfouling materials, have a high target capacity, and provide solution-like hybridization thermodynamics. With these considerations in mind, hydrogels are proving to be excellent substrates for biomolecule capture and quantification.

Hydrogels are a class of biofriendly materials that characteristically retain water, allowing biological interactions to occur in three-

* To whom correspondence should be addressed. Phone: 617-253-4534. Fax: 617-258-5042. E-mail: pdoyle@mit.edu.

(1) Lamb, J.; Crawford, E. D.; Peck, D.; Modell, J. W.; Blat, I. C.; Wrobel, M. J.; Lerner, J.; Brunet, J.-P.; Subramanian, A.; Ross, K. N.; Reich, M.; Hieronymus, H.; Wei, G.; Armstrong, S. A.; Haggarty, S. J.; Clemons, P. A.; Wei, R.; Carr, S. A.; Lander, E. S.; Golub, T. R. *Science* **2006**, *313*, 1929–1935.
(2) Calin, G. A.; Ferracin, M.; Cimmino, A.; Di Leva, G.; Shimizu, M.; Wojcik, S. E.; Iorio, M. V.; Visone, R.; Sever, N. I.; Fabbri, M.; Iuliano, R.; Palumbo, T.; Pichiorri, F.; Roldo, C.; Garzon, R.; Sevignani, C.; Rassenti, L.; Alder, H.; Volinia, S.; Liu, C.-g.; Kipps, T. J.; Negrini, M.; Croce, C. M. *N. Engl. J. Med.* **2005**, *353*, 1793–1801.
(3) Cummins, J. M.; Yiping He, Y.; Leary, R. J.; Pagliarini, R.; Diaz, L. A., Jr.; Sjoblom, T.; Barad, O.; Bentwich, Z.; Szafranska, A. E.; Labourier, E.; Raymond, C. K.; Roberts, B. S.; Juhl, H.; Kinzler, K. W.; Vogelstein, B.; Velculescu, V. E. *Proc. Natl. Acad. Sci. U.S.A.* **2006**, *103*, 3687–3692.
(4) Jay, C.; Nemunaitis, J.; Chen, P.; Fulgham, P.; Tong, A. W. *DNA Cell Biol.* **2007**, *26*, 293–300.
(5) Volinia, S.; Calin, G. A.; Liu, C.-G.; Ambs, S.; Cimmino, A.; Petrocca, F.; Visone, R.; Iorio, M.; Roldo, C.; Ferracin, M.; Prueitt, R. L.; Yanaihara, N.; Lanza, G.; Scarpa, A.; Vecchione, A.; Negrini, M.; Harris, C. C.; Croce, C. M. *Proc. Natl. Acad. Sci. U.S.A.* **2006**, *103*, 2257–2261.
(6) Nolan, J. P.; Sklar, L. A. *Trends Biotechnol.* **2002**, *20*, 9–12.
(7) Finkel, N. H.; Lou, X.; Wang, C.; He, L. *Anal. Chem.* **2004**, *76*, 352A–359A.
(8) Braeckmans, K.; De Smedt, S. C.; Leblans, M.; Pauwels, R.; Demeester, J. *Nat. Rev. Drug Discovery* **2002**, *1*, 447–456.
(9) Fulton, R. J.; McDade, R. L.; Smith, P. L.; Kienker, L. J.; Kettman, J. J. R. *Clin. Chem.* **1997**, *43*, 1749–1756.
(10) Ramaswamy, S.; Tamayo, P.; Rifkin, R.; Mukherjee, S.; Yeang, C. H.; Angelo, M.; Ladd, C.; Reich, M.; Latulippe, E.; Mesirov, J. P.; Poggio, T.; Gerald, W.; Loda, M.; Lander, E. S.; Golub, T. R. *Proc. Natl. Acad. Sci. U.S.A.* **2001**, *98*, 15149–15154.
(11) Halperin, A.; Buhot, A.; Zhulina, E. B. *Biophys. J.* **2005**, *89*, 796–811.
(12) Vainrub, A.; Pettitt, B. M. *Biopolymers* **2003**, *68*, 265–270.

10.1021/ac9005292 CCC: $40.75 
Published on Web 05/12/2009

dimensional space. In comparison to glass substrates, hydrogel materials (e.g., poly(ethylene glycol), PEG) are nonfouling, thus limiting nonspecific interactions, and can be derived from a broad list of precursors. Moreover, although hybridization is dramatically inhibited on solid surfaces,[13] Mirzabekov's group has shown that nucleic acid hybridization in gels closely resembles that in solution.[14] Furthermore, by collecting fluorescence from a three-dimensional volume as opposed to a two-dimensional plane, a greater number of fluorophores can be captured to provide enhanced sensitivity. It was demonstrated that gel substrates exhibit better sensitivity and a higher capacity than their glass counterparts for both nucleic acids[15] and proteins.[16] Although gels have been used successfully for planar arrays, the application of hydrogel for particle arrays is very limited.

In planar or particle arrays, solid or gel-based, an understanding of the kinetics for target capture can be used to design and optimize assays. The kinetics of biomolecule capture involves mass transport (convection and/or diffusion) of target molecules to an active substrate and subsequent chemical reaction with an immobilized probe. Hybridization kinetics have been studied and modeled extensively over a variety of substrates and conditions. Analyses include capture on solid substrates with forced convection[17−19] or in stagnant fluids[20−22] and also capture in hydrogel substrates.[19,23] Typically, analytical solutions can only be found for specific regimes where the nonlinear, coupled equations governing transport can be simplified. Furthermore, although modeling has been accomplished for particle arrays[24] and planar hydrogel arrays,[18,19,23] modeling has not been done for *hydrogel particle* arrays.

Recently, we developed a method for molecular screening based on multifunctional encoded hydrogel particles.[25] These particles are generated using flow lithography—a process that allows for the rapid generation of morphologically complex, monodisperse (coefficients of variation <2%) particles from a broad range of precursor materials.[26,27] For bioassays, we use PEG precursors that cross-link upon UV exposure to form encoded particles composed of a porous hydrogel network. Encoded particles are incubated with a sample containing unknown species and subsequently scanned for fluorescence in a flow-through device where barcodes are read and the corresponding targets quantified. Our multiplexing technology provides a virtually unlimited number of codes, single-color, rapid flow-through scanning, and the ability to detect several targets on single particles.[25] Although we demonstrated proof-of-concept multiplexed nucleic acid detection, the performance of our system was not previously assessed. Here, we elucidate the parameters dictating assay sensitivity and subsequently optimize particle and assay design to demonstrate high-performance nucleic acid quantification.

## MATERIALS AND METHODS

**Fabrication and Assembly of Microfluidic Devices.** Microfluidic channels were molded on 4 in. silicon wafers using standard soft lithography. Briefly, SU-8 photoresist (MicroChem) was spin-coated on a clean silicon wafer for 30 s at a speed selected to obtain the desired layer thickness. After a brief 65 °C prebake on a hot plate, the wafer was exposed to UV irradiation through a transparency mask. The photoresist was then postbaked at 95 °C, and subsequently, unexposed photoresist was removed using a developer. Poly(dimethylsiloxane) (PDMS) (Sylgard 184, Dow Corning) was mixed at a base to curing agent ratio of 10:1. The elastomer was degassed for 30 min and poured over the silicon wafer mold. The PDMS was then cured overnight at 65 °C. Holes for external connection were punched out using a blunt-ended syringe needle. Glass slides were coated with PDMS and partially cured (for 20 min at 65 °C). Cleaned channels were then placed on the slides and contact-sealed. The assembled devices were then baked for an additional 45 min at 65 °C.

**Microscope Setup.** All experiments were performed using an Axiovert 200 (Zeiss) inverted microscope with a VS25 shutter system (UniBlitz) in place to precisely control UV exposure dose. A 100 W HBO mercury lamp in conjunction with wide-range excitation UV filter (11000v2:UV, Chroma) provided irradiation of the desired wavelength. Transparency masks designed using Autocad were printed by CAD/Art Services, Inc. (Bandon, OR) at 10 000 dpi resolution. Each mask was designed to be circular, 2.5 cm in diameter, with features typically printed no more then 0.5 cm radially from the mask center. During an experiment, a mask was sandwiched between two 25 mm circular glass coverslips (VWR), placed in the first slot of the filter slider bar, and secured with an O-ring. The filter slider was then positioned in the field-stop position of the microscope. Images were processed using NIH Image.

**Particle Synthesis Using Stop-Flow Lithography.** Precursor solutions consisted of blends of poly(ethylene glycol) diacrylate (PEG-DA, $M_n$ = 700, ~70 cP at 25 °C, Aldrich) and PEG ($M_w$ = 200, ~50 cP at 25 °C, Aldrich) in 35% 3× Tris−EDTA buffer (pH = 8.0, EMD) with 5% Darocur 1173 photoinitiator (Alrich). When applicable, DNA probe modified with an acrydite group (IDT) was included at concentrations ranging from 10 to 100 μM. The sequences of the oligomers used are given in Table 1. These precursor samples were loaded into channels using pipet tips (200 μL, Molecular BioProducts), connected with rubber tubing (Tygon) to a common pressure source (regulated by a pressure valve, Controlair Inc.). The tips were filled with ~100 μL of polymer and inserted into the channel inlet ports. A three-



(13) Levicky, R.; Horgan, A. *Trends Biotechnol.* **2005**, *23*, 143–149.
(14) Fotin, A. V.; Drobyshev, A. L.; Proudnikov, D. Y.; Perov, A. N.; Mirzabekov, A. D. *Nucleic Acids Res.* **1998**, *26*, 1515–1521.
(15) Sorokin, N. V.; Chechetkin, V. R.; Pan'kov, S. V.; Somova, O. G.; Livshits, M. A.; Donnikov, M. Y.; Turygin, A. Y.; Barsky, V. E.; Zasedatelev, A. S. *J. Biomol. Struct. Dyn.* **2006**, *24*, 57–66.
(16) Zubtsov, D. A.; Savvateeva, E. N.; Rubina, A. Y.; Pan'kov, S. V.; Konovalova, E. V.; Moiseeva, O. V.; Chechetkin, V. R.; Zasedatelev, A. S. *Anal. Biochem.* **2007**, *368*, 205–213.
(17) Squires, T. M.; Messinger, R. J.; Manalis, S. R. *Nat. Biotechnol.* **2008**, *26*, 417–426.
(18) Zubtsov, D. A.; Ivanov, S. M.; Rubina, A. Y.; Dementieva, E. I.; Chechetkin, V. R.; Zasedatelev, A. S. *J. Biotechnol.* **2006**, *122*, 16–27.
(19) Sorokin, N. V.; Yurasov, D. Y.; Cherepanov, A. I.; Kozhekbaeva, J. M.; Chechetkin, V. R.; Gra, O. A.; Livshits, M. A.; Nasedkina, T. V.; Zasedatelev, A. S. *J. Biomol. Struct. Dyn.* **2007**, *24*, 571–578.
(20) Gadgil, C.; Yeckel, A.; Derby, J. J.; Hu, W. S. *J. Biotechnol.* **2004**, *114*, 31–45.
(21) Erickson, D.; Li, D. Q.; Krull, U. J. *Anal. Biochem.* **2003**, *317*, 186–200.
(22) Bishop, J.; Chagovetz, A. M.; Blair, S. *Biophys. J.* **2008**, *94*, 1726–1734.
(23) Livshits, M. A.; Mirzabekov, A. D. *Biophys. J.* **1996**, *71*, 2795–2801.
(24) Henry, M. R.; Wilkins Stevens, P.; Sun, J.; Kelso, D. M. *Anal. Biochem.* **1999**, *276*, 204–214.
(25) Pregibon, D. C.; Toner, M.; Doyle, P. S. *Science* **2007**, *315*, 1393–1396.
(26) Dendukuri, D.; Pregibon, D. C.; Collins, J.; Hatton, T. A.; Doyle, P. S. *Nat. Mater.* **2006**, *5*, 365–369.
(27) Dendukuri, D.; Gu, S. S.; Pregibon, D. C.; Hatton, T. A.; Doyle, P. S. *Lab Chip* **2007**, *7*, 818–828.

**Table 1. List of Nucleic Acid Probes and Targets Used in This Work**[a]

DNA Probes

| name | sequence and modifications |
|---|---|
| $P_{comp}$ | 5′-acrydite-FITC−GGA TGG GGA CTG TGG GTA GAT AGG GGA ACA ATG AGA GTC AAC TCA GGC TA-3′ |
| $P_{7a}$ | 5′-acrydite−AAC TAT ACA ACC TAC TAC CTC A-3′ |
| $P_{7b}$ | 5′-acrydite−AAC CAC ACA ACC TAC TAC CTC A-3′ |
| $P_{7c}$ | 5′-acrydite−AAC CAT ACA ACC TAC TAC CTC A-3′ |
| $P_{7d}$ | 5′-acrydite−AAC TAT GCA ACC TAC TAC CTC T-3′ |

DNA/RNA Targets

| name | sequence and modifications |
|---|---|
| $T_{20}$ | 5′-biotin−CTC ATT GTT CCC CTA TCT AC-3′ |
| $T_{50}$ | 5′-biotin−TAG CCT GAG TTG ACT CTC ATT GTT CCC CTA TCT ACC CAC AGT CCC CAT CC-3′ |
| $T_{100}$ | 5′-biotin−[TAG CCT GAG TTG ACT CTC ATT GTT CCC CTA TCT ACC CAC AGT CCC CAT CC]$_2$-3′ |
| $T_{200}$ | 5′-biotin−[TAG CCT GAG TTG ACT CTC ATT GTT CCC CTA TCT ACC CAC AGT CCC CAT CC]$_4$-3′ |
| $T_{7a}$ | 5′-UGA GGU AGU AGG UUG UAU AGU U-3′ |

[a] For composition studies, the DNA probe $P_{comp}$ was used with DNA targets $T_{20}$−$T_{200}$. For sensitivity and specificity studies, the probes $P_{7a}$−$P_{7d}$ were used with RNA target $T_{7a}$.



way solenoid valve (Burkert) allowed for the oscillation between pressurized (typically ~3 psi, high velocity) and ambient-pressure (no flow) states as shown in Figure 1. A valving system with resistive elements (filter-top pipet tips, Molecular BioProducts) and needle valves (Swagelok) provided independent control of the stream widths. Visual alignment for polymerization was achieved using a CCD camera (KPM1A, Hitachi) with NIH Image software. Control of flow (via solenoid valve) and UV exposure doses was accomplished using a custom-written script in LabView to allow continuous synthesis of particles. Typical times for flow, hold, UV exposure, and hold were 500, 300, 75, and 125 ms, respectively.

**Hybridization Assay.** All assays were carried out using a hybridization buffer containing either 0.2 M (composition study) or 0.5 M NaCl (sensitivity/specificity studies) in 1× Tris−EDTA (pH = 8) with 0.05% Tween-20. The samples were incubated in 0.65 mL Eppendorf tubes at the desired temperature and duration using a thermomixer (Quantifoil Rio) with a mixing speed of 1800 rpm.

**Labeling Biotinylated Targets.** After hybridization, particles were rinsed 2× with PBS containing 0.05% Tween-20 (PBST). Then, streptavidin-r-phycoerythrin reporter (SAPE) was diluted 1:50 in PBST and added to obtain a final dilution of 1:500. The samples were then incubated at 37 °C for 30 min with mixing at 1800 rpm. Before imaging, particles were rinsed 2× with PBST and then 1× in PTET (5× Tris−EDTA buffer, pH = 8, with 25% PEG ($n$ = 200) and 0.05% Tween-20).

**Imaging for Quantitative Analysis.** Rinsed particle samples were pipetted into glass slides and sealed with a coverslip, which was then mounted on a Zeiss Axiovert 200 microscope. We used NIH Image to visualize images captured from an EB-CCD camera (C7190-20, Hamamatsu) mounted to the sideport of the microscope with camera settings of 10, 1.6, and 9.7 for gain, offset, and sensitivity, respectively. We used a Zeiss A-Plan 10× objective (NA = 0.25) and an Exfo X-Cite illumination source (series 120) at the highest setting. Movies taken in NIH Image at 20 frames/s over 10 frames were averaged and saved as a single image. These images were analyzed using ImageJ software.

## RESULTS AND DISCUSSION

**Modeling Hybridization.** In order to optimize hybridization assays, it is essential to determine how system parameters dictate assay kinetics and sensitivity. As stated earlier, kinetic modeling has not been done for assays involving porous particles, particularly hydrogels. To better understand hybridization kinetics using encoded hydrogel particles, we develop a quantitative model using dimensional analysis to simplify the problem and identify important parameters.

The encoded particles used in our system typically bear a barcode region, an inert region, and one or multiple probe regions. For this exercise, we consider particles bearing a single probe region flanked by two inert regions (Figure 1). Such particles are synthesized using stop-flow lithography[27] with a three-inlet microfluidic device. In order to have precise control over the probe-region width, we utilize a custom-built valving system to independently adjust the pressure of each inlet—this allows us to set the relative width of each stream flowing along the channel (Figure 1a). In an assay, particles are hybridized in a sample containing tagged or fluorescently labeled targets at unknown concentrations, with continuous mixing to facilitate mass transfer. The porous nature of our particles allows targets to diffuse and react deep within the particle interior, as shown by the thick, bright edges on the probe region of the particle in Figure 1b. After hybridization, particles are scanned for fluorescence along their length with their broad face down (Figure 1b). In our system, fluorescence is captured through the entire depth of the particle for maximum sensitivity. The "signal" obtained for a scan represents the fluorescent intensity at the center of the probe region minus the average background fluorescence measured in the inert regions of the particle as shown in Figure 1c. We are interested in developing a model that will allow us to understand and predict such signals with a given incubation time and initial target concentration.

For this analysis, we consider rectangular particles ($2L \times 2W$) of extruded thickness $2l$ with a single probe-region stripe (of thickness $2d$) flanked by two inert gel regions serving as negative controls, as shown in Figure 1d. We locate the origin of the coordinate system at the center of the particle. Due to the symmetry of the problem, we designate our region of interest to be the volume contained by $(x, y, z) \geq 0$ (Figure 1d).

During hybridization, target oligonucleotides (denoted $T_s$ in solution and T within the particles) diffuse into the particle surface and bind with incorporated probes P to form complexes TP (Figure 1e). The particles are assumed to be homogeneous with a target diffusivity in the gel denoted $D_{gel}$. We consider a sample of volume $V_s$ where there are $N_p$ particles each with a probe-region volume of $V_p$. The dissociation constant for a target−probe complex is given by $K_d = k_d/k_a$ where $k_d$ and $k_a$ are the first-order dissociation and second-order association rate constants for a given target−probe pair, respectively.

We assume that the solution is well-mixed such that the concentration of target is homogeneous throughout the solution. Thus, while species in the particle can vary by location, **r**, and time, $t$ (i.e., [T], [P], [TP] = $f(\mathbf{r}, t)$), the target in solution only varies with

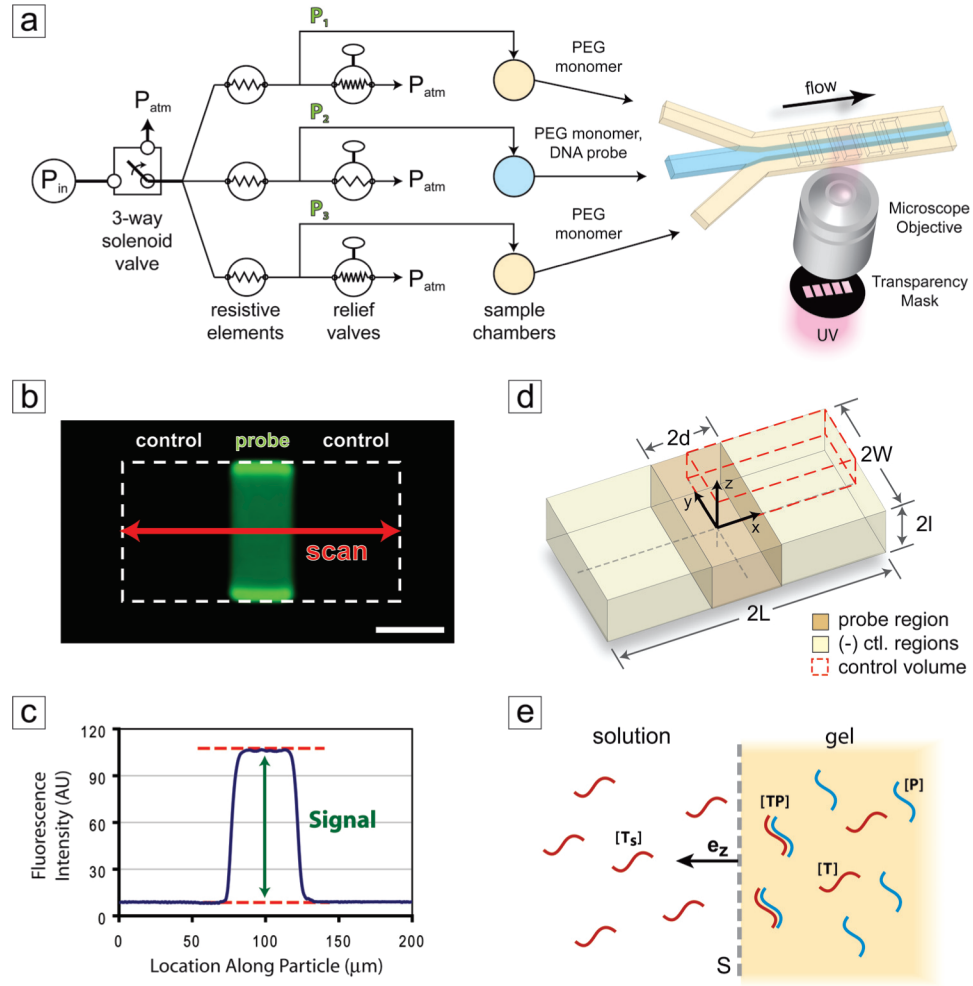


**Figure 1.** (a) Schematic of particle synthesis. Three streams with controllable widths are flowed along a microfluidic channel, stopped, and polymeric particles are formed when bursts of UV light cross-link the monomer precursors. (b) Fluorescence image of a particle after hybridization with fluorescent target. The particle, with a probe region flanked by two inert regions, is outlined with a dotted white line. (c) Scan of fluorescence along the length of the particle shown in panel b with the measured signal taken as the probe-region fluorescence minus background fluorescence. (d) Particle design for modeling. The origin of the coordinate system is designated at the center of the particle. (e) Target oligonucleotides ($T_s$ in solution, T within particles) in solution diffuse to the particle and through the porous interior, binding with incorporated probes P to form complexes TP. Scale bar is 50 $\mu$m.



time ($[T_s] = [T_s](t)$). It is also important to note that the sample volume is several orders of magnitude larger than the total particle volume (the ratio of sample/particle volume is typically $\sim 10^3$), so it can be assumed that the concentration of target in solution ($T_s$) is unaffected by the presence of target within the particles ($T$). The equations governing the conservation of species in this problem are given by

$$\frac{\partial[T]}{\partial t} = D_{gel}\nabla^2[T] - k_a[P][T] + k_d[TP] \quad (1)$$

$$\frac{\partial[P]}{\partial t} = -k_a[P][T] + k_d[TP] \quad (2)$$

$$[TP] = [P]_o - [P] \quad (3)$$

$$V_s\frac{d[T_s]}{dt} = -N_p\int_S [(D_{gel}\nabla[T])\cdot\mathbf{n}]\, dS \quad (4)$$

where $\mathbf{n}$ is a unit vector normal to the particle surface, $S$. Initially ($t = 0$), all target is in solution and unbound probe is evenly distributed throughout the particle probe region (with no probe in the inert regions). The boundary conditions for target come from symmetry, giving zero net flux through the center of the particle and concentration matching at the particle/solution interface (i.e., a partition coefficient of one as has been used for other gel systems[23]).

Unfortunately, these equations are nonlinear and coupled. As set up, it is not possible to obtain a general analytical solution. However, we will show that in a specific regime, which is relevant to most assays, the system can be simplified to a one-dimensional problem and solved analytically.

Scaling arguments can be made to reduce the complexity of this problem. Specifically, we are interested in dimensionless groups that describe (1) the ratio of target to probe molecules ($\gamma = [T_s]_o V_s/([P]_o N_p V_p)$), (2) the rate of association versus diffusion which is given by the Damköhler number ($Da = k_a[P]_o/(D_{gel}/l^2)$), and (3) the relative strength of hybridization ($\kappa = K_d/[T_s]_o$).

We consider the reaction of short oligonucleotides (~20 bp) at moderate to low levels (<500 × $10^{-18}$ mol). In this scenario (with a typical particle design), probe is in great excess ($\gamma \ll 1$), the rate of association is much greater than diffusion ($Da$

$\gg 1$), and hybridization is very strong at the initial target concentration ($\kappa \ll 1$), specifically $\gamma \sim 2 \times 10^{-2}$, $Da \sim 4 \times 10^{2}$, and $\kappa \sim 2 \times 10^{-3}$. These values were found using typical assay parameters[23] of $k_a \sim 5 \times 10^{6}$ M s$^{-1}$, $k_d \sim 10^{-7}$ s$^{-1}$, $[P]_o \sim 5 \times 10^{-6}$ M, $[T_s]_o \sim 10^{-11}$ M, $V_s \sim 5 \times 10^{-5}L$, $N_p \sim 30$, $V_p \sim 15 \times 10^{-11}L$, $2l \sim 25 \times 10^{-6}$ m, and $D_{gel} \sim 10^{-11}$ m$^2$ s$^{-1}$.

With $Da \gg 1$, the penetration distance for target molecules into the probe region can be approximated as $l/Da^{1/2} \sim 0.5\ \mu$m, which is orders of magnitude smaller than the other length scales in the problem ($W$, $L$, $l$, and $d$). This implies that in the probe region, mass transport is occurring close to the particle surface, creating a core−shell profile for bound target. The large $Da$ also implies that diffusion of targets through the inert gel regions toward the interior interfaces of the probe region will be much slower than binding at those interfaces. These considerations justify simplification to one-dimension (1D), where we can model the system as a semi-infinite slab, ignoring the inert regions of the particles and any edge effects. We will find a solution to this 1D problem and apply it across the exposed probe-region surface, which has an area $A_p$, keeping the $z$-dimension as our single coordinate.

Although eqs 2 and 3 remain unchanged with 1D simplification, eqs 1 and 4 become

$$\frac{\partial [T]}{\partial t} = D_{gel}\frac{\partial^2 [T]}{\partial z^2} - k_a[P][T] + k_d[TP] \tag{5}$$

$$V_s\frac{d[T_s]}{dt} = -N_p A_p D_{gel}\left.\frac{\partial [T]}{\partial z}\right|_{z=l} \tag{6}$$

The initial conditions are given by

$$[T_s](t=0) = [T_s]_o \tag{7}$$

$$[T](z,0) = [TP](z,0) = 0 \tag{8}$$

$$[P](z,0) = [P]_o \tag{9}$$

and boundary conditions, remembering that we are modeling the system as a semi-infinite slab, by

$$[T](z=0,t) = 0 \tag{10}$$

$$[T](z=l,t) = T_s(t) \tag{11}$$

To find the time scale of the problem, we consider the scenario that leads to maximum signal, which in the case of excess probe happens when all of the target is captured in the particles. This time is associated with eq 6. We can scale the length and concentrations using $\eta = Da^{1/2}(l-z)/l$, $\tilde{T}_s = [T_s]/[T_s]_o$, and $\tilde{T} = [T]/[T_s]_o$. We can then group all terms on the left-hand side and choose a time scale that makes all terms in the equation of order one. The resulting dimensionless time governing target depletion from solution is

$$\tau = t/\left(\frac{V_s}{N_p A_p (D_{gel}k_a[P]_o)^{\frac{1}{2}}}\right) \tag{12}$$

It is important to notice that this time scale governing $T_s$ is of order $10^3$ s, which is much longer than the time scale governing species evolution in eqs 1−3 ($k_a[P]_o \sim 1$ s). Therefore, a pseudo-steady-state approximation can be made for T, P, and TP.

Target−probe complex can be scaled using $\widetilde{TP} = [TP]/([T_s]V_s/V_p)$, which represents the concentration relative to that if all target from solution was hybridized homogeneously throughout the total probe-region volume, whereas probe is scaled naturally as $\tilde{P} = [P]/[P]_o$. We now scale the four governing equations using the time scale in eq 12 and the scalings for length and concentrations given above. In each equation, we can group parameters and use dimensional analysis to neglect terms that are not significant. In particular, we can solve for [P] in eq 3, substitute it into eq 5, and apply the appropriate scaling. Realizing that the lumped parameters of the resulting equation, $N_p A_p l/(Da^{1/2})$, $V_s[T_s]_o/(N_p V_p [P]_o)$, and $K_d/[P]_o$ are all $\ll 1$, we can neglect several terms from the equation to find

$$0 = \frac{\partial^2 \tilde{T}}{\partial \eta^2} - \tilde{T} \tag{13}$$

which has a general solution of $\tilde{T} = C_1 e^{-\eta} + C_2 e^{\eta}$, where $C_1$ and $C_2$ are parameters to be found using the boundary conditions. In this regime where $Da \to \infty$ and $\tilde{T} \to 0$ at $\eta \to \infty$, our scaled boundary conditions for this 1D case become

$$\tilde{T}(\eta \to \infty, \tau) = 0 \tag{14}$$

$$\tilde{T}(\eta = 0, \tau) = \tilde{T}_s(\tau) \tag{15}$$

Applying these boundary conditions to the general solution, we find that the concentration of target within the particle is given by

$$\tilde{T} = \tilde{T}_s e^{-\eta} \tag{16}$$

This solution can be applied to eq 6, which in dimensionless form becomes

$$\frac{d\tilde{T}_s}{d\tau} = \left.\frac{\partial \tilde{T}}{\partial \eta}\right|_{\eta=0} = -\tilde{T}_s \tag{17}$$

The general solution to eq 17 is $\tilde{T}_s = C_1 e^{-\tau}$ where $C_1$ is a constant to be determined. Using the scaled initial condition of $\tilde{T}_s(\tau = 0) = 1$ from eq 8 with this general solution, we find that the depletion of target from solution is governed by

$$\tilde{T}_s = e^{-\tau} \tag{18}$$

This result suggests the exponential decay of target from solution, governed by a time scale dependent on probe concentration, sample volume, particle surface area, and diffusivity of target in the gel particles. The rate at which target depletes from solution is inversely related to the rate of target−probe complex formation in the particles. Assuming an even distribution of captured target molecules across the probe-

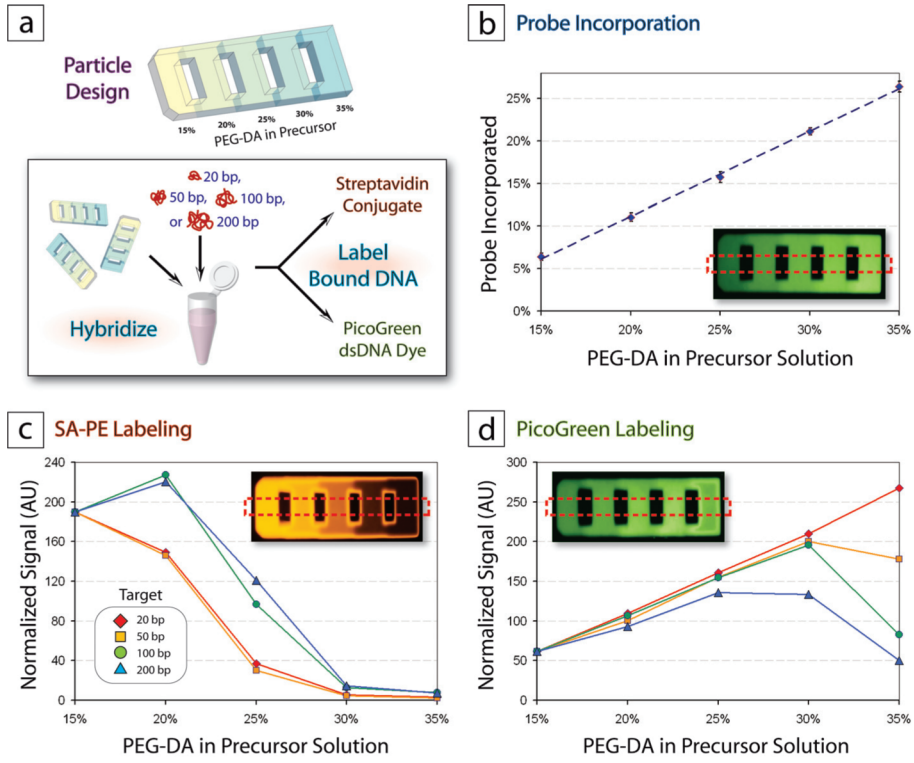


**Figure 2.** Particle composition study. (a) Pentafunctional particles made from monomer solutions containing 15−35% PEG-DA were investigated for probe incorporation (b) and hybridization signal using two methods of fluorescent detection (c and d). The error bars shown in panel b represent the standard deviation over three measurements. In panels c and d, fluorescent scans along the particles were normalized to the intensity measured for the 15% PEG-DA regions in order to show penetration trends for the two labeling schemes. Particles have dimensions of 400 × 100 × 30 $\mu m^3$.

region surface for all particles in the assay, we can estimate the fluorescent signal intensity ($I$) seen on the particles using

$$I = \frac{F_e V_s [T_s]_o (1 - e^{-\tau})}{N_p A_p} \quad (19)$$

where $F_e$ is a signal efficiency factor (with units AU $m^2$/mol) that takes into account fluorophore and detector efficiencies as well as the number of hybridization surfaces through which signal is measured (which is two in the case of our particles). This result indicates that for maximum sensitivity, long hybridization times should be used with minimum particle numbers and probe-region surface while for the fastest kinetics, assays should be in small volumes with maximum probe concentration, diffusivity, and association kinetics.

**Investigation of Particle Composition.** It is clear from the time scale shown in eq 12 that the diffusivity of targets in the gel matrix, $D_{gel}$, and also the concentration of probe incorporated, $[P]_o$, will play a major role in determining the system kinetics. Diffusivity is directly related to the porosity of a gel matrix, which can be varied by altering the composition of prepolymer solutions. Pore size can be tuned efficiently using blends of reactive and inert species, forming a semi-interpenetrating network[28] (semi-IPN). Although larger pores will allow faster transport, it is also expected that they will lead to a decrease in probe incorporation efficiency and particle rigidity. In order to investigate the effects of prepolymer composition, we used a semi-IPN consisting of both reactive PEG-DA ($M_n$ = 700) and inert PEG ($M_w$ = 200) mixed at different ratios.

To efficiently study the effects of particle composition on probe incorporation and hybridization signal, we synthesized pentafunctional "ladder" particles using stop-flow lithography.[27] As shown in Figure 2a, each rung of the ladder had a unique composition. All prepolymer solutions contained a total of 60% PEG (PEG-DA + PEG), with the amount of PEG-DA ranging from 15% to 35%. In each monomer solution, we used 5% Darocur 1173 and 35% of 3× TE. The monomer solutions were mixed at 9:1 with a 50 bp DNA probe, which was modified with a fluorescein group to assess incorporation efficiency. The final DNA concentration in the monomer blends was 5 $\mu$M.

In addition to probe incorporation efficiency, particles were also assessed for hybridization signal obtained after incubation with targets varying in length from 20 to 200 bp. For these hybridization studies, we used two different target labeling schemes based on SAPE or PicoGreen as fluorescent reporters. These two reporters were chosen due to their dramatic difference in size. Whereas PicoGreen is a small, DNA-binding cyanine dye on the order of 1 nm, streptavidin and r-phycoerythrin are both proteins with diameters on the order of 4 and 10 nm, respectively.[29,30] Although SAPE is a very efficient reporter for fluorescent detection, it is also one of the largest, making it a good test of the upper limit for target labeling. Alternatively, fluorescently labeled targets

(28) Witte, R. P.; Blake, A. J.; Palmer, C.; Kao, W. J. *J. Biomed. Mater. Res., Part A* **2004**, *71*, 508–518.

(29) Green, N. M. *Methods Enzymol.* **1990**, *184*, 51–67.

(30) MacColl, R.; Eisele, L. E.; Williams, E. C.; Bowser, S. S. *J. Biol. Chem.* **1996**, *271*, 17157–17160.

can be directly captured and detected without the use of a reporter, as shown in previous work[25] and also in the model validation experiments discussed later.

**Probe Incorporation Efficiency.** The incorporation of fluorescent probe at various precursor compositions is shown in Figure 2b. To find values of incorporated probe relative to that in precursor, the fluorescence at each particle composition was normalized using the fluorescence obtained from particles made using 60% PEG-DA, which were assessed immediately after synthesis. At this high concentration of PEG-DA, it can be assumed that nearly all of the 50 bp ($r_g \sim 4$ nm) probe is incorporated within the particles, either by covalent linkage or physical entrapment (as fully cross-linked PEG-DA ($M_n = 700$) is known to have a pore size of ~1 nm[31,32]).

The results of this analysis show that the amount of reactive species in precursor solutions affect probe incorporation in a linear fashion over the compositions studied, with incorporations ranging from ~5% to 25%. This trend is expected as the propagation rate is linear with respect to double-bond concentration for multifunctional, reactive monomers.[33] Although it is by no means a limitation of our system, it is possible that the incorporation efficiency may be increased by matching the reaction rates of the monomer and probe species, which in this experiment were acrylates and methacrylates, respectively. It is known that acrylates react faster than methacrylates, so it is possible that if methacrylated monomers or acrylated probes were used, the probe incorporation would be higher.

**Target Hybridization Signal.** We expected that changing the particle composition would alter the resulting pore size. To study this in the context of DNA hybridization, we performed assays using biotinylated DNA targets with varying sizes of 20, 50, 100, and 200 bp. Using the Kratky−Porod equation,[34] we can estimate that oligonucleotides of these lengths have radii of gyration ($r_g$) on the order of 2, 4, 7, and 10 nm with the ionic strength used (0.1 M). It is important to realize that the use of polymer targets (such as DNA) will not provide a direct measurement of the hydrogel pore size as these semiflexible polymer chains can traverse the gel via reptation.

Particles were hybridized with each target present at great excess (1 $\mu$M) for 90 min and assessed for fluorescence using both labeling methods (Figure 2, parts c and d). The absolute values of fluorescent signal were dependent on target length, which is expected as both length and secondary structure are known to alter association rates.[35] For this reason, signals from each data set were normalized using a scale factor to match the intensities of the 15% PEG-DA regions over all target lengths. This is done to emphasize trends with respect to particle composition.

In both labeling schemes, the reporter entities (SAPE or PicoGreen) are added after hybridization. As such, the reporters may be size-excluded from regions of the particle where their size is larger than the pore size. This is the case for the bulky SAPE reporter, as shown in Figure 2c. Above a composition of 25% PEG-DA, SAPE is excluded from the particle interior; this is shown by a dramatic decrease in hybridization signal with all target sizes. This suggests that particle compositions of less than 25% PEG-DA must be used for SAPE-based labeling schemes.

In order to get a better understanding of DNA hybridization throughout the particles, we used PicoGreen—a DNA dye that has ~100× fluorescent enhancement when bound to dsDNA (or DNA/RNA) versus ssDNA. The small size of this dye allows it to penetrate all regions of the particle. As shown in Figure 2d, the 20 bp target signal has an intensity profile mimicking that of probe incorporation in Figure 2b. This suggests that the small, 20 bp target can completely penetrate all regions of the particle, hybridizing throughout in the 90 min incubation period. The larger targets show this trend for lower PEG-DA concentrations, but it starts to deviate with smaller pore sizes. For instance, the 50 and 100 bp target signals start diminishing at 30% PEG-DA, whereas the 200 bp target shows decrease beginning at 25%. These results show that, as expected, the particle composition can be tuned to selectively inhibit penetration of larger oligonucleotide targets.

In selecting an "optimized" particle composition for general assay use, we chose the composition of 20% PEG-DA. This composition allows use of both fluorescent labeling schemes and ensures that particles are mechanically robust (instances of morphological deformation were observed for some of the 15% PEG-DA particle regions). As shown in Figure 2b, particles made from this composition retain ~11% of the probe included in the precursor solution.

**Experimental Validation of Model.** We investigated the validity of our model by performing kinetic studies using particles similar to that shown schematically in Figure 1 with varying probe concentrations (from 1 to 5 $\mu$M), probe-region surface areas ($2d$ from 45 to 80 $\mu$m), and particle numbers (from 20 to 40). In each case, we incubated distinct particle samples with 500 amol of fluorescein-labeled target at room temperature. At various time points, particles from a sample were measured for fluorescence. We plotted the raw data as cumulative fluorescent intensity over all particles, as our model predicts the cumulative target loss from solution. As can be seen in Figure 3a, the data covers a widespread of fluorescent intensity over incubation time.

To evaluate our model, we scaled time using the relationship in eq 12 and the signal from eq 19 using

$$\tilde{I}N_p = \frac{IA_p}{F_e V_s [T_s]_o} N_p = 1 - e^{-\tau} \qquad (20)$$

We plotted the scaled data (Figure 3b) to find that it collapses nicely on a similar trend. We fit the parameters $k_a D_{gel}$ and $F_e$ to find a curve that best fit the data. Using these parameters, we compared the experimentally observed fluorescent signals with signals predicted from our model as shown in Figure 3b on the right. The model agreed with experimental data over the entire range of fluorescent intensities studied, thus validating our model for this specific hybridization regime.

**Investigation of Sensitivity.** With a quantitative model in place to understand hybridization in a rare-target regime, we assessed the sensitivity of our system over a range of hybridization times. As an optimized design, we chose particles with 20% PEG-DA composition (which gives large pores with suitable particle


(31) Mellott, M. B.; Searcy, K.; Pishko, M. V. *Biomaterials* **2001**, *22*, 929–941.
(32) Cruise, G. M.; Scharp, D. S.; Hubbell, J. A. *Biomaterials* **1998**, *19*, 1287–1294.
(33) Andrzejewska, E. *Prog. Polym. Sci.* **2001**, *26*, 605–665.
(34) Meagher, R. J.; Won, J. I.; McCormick, L. C.; Nedelcu, S.; Bertrand, M. M.; Bertram, J. L.; Drouin, G.; Barron, A. E.; Slater, G. W. *Electrophoresis* **2005**, *26*, 331–350.
(35) Gao, Y.; Wolf, L. K.; Georgiadis, R. M. *Nucleic Acids Res.* **2006**, *34*, 3370–3377.

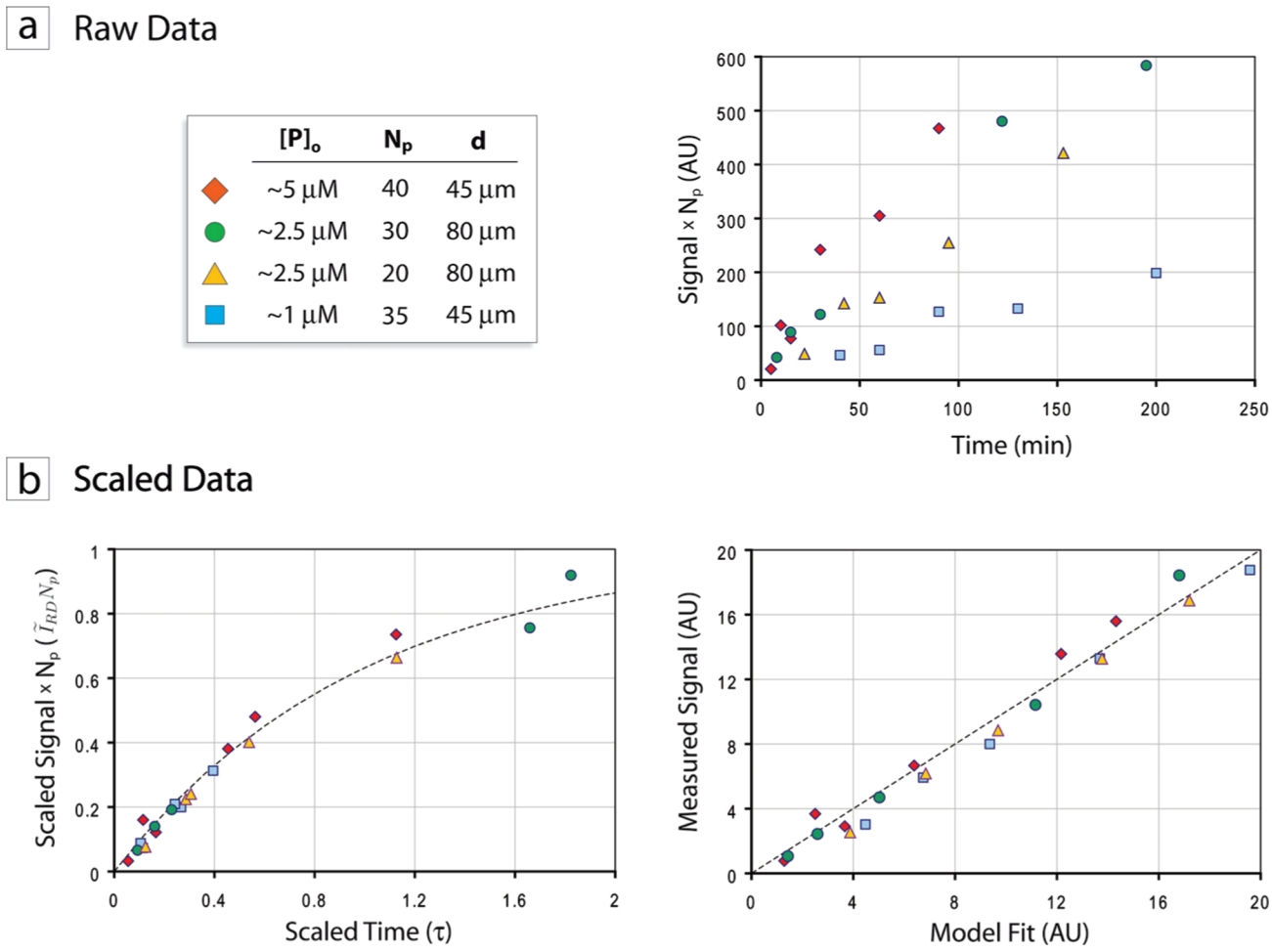


**Figure 3.** Validation of model predictions. Particles with varying probe concentrations ($[P]_o$), stripe width ($d$), and numbers ($N_p$) were incubated with 500 amol of complementary, fluorescein-labeled target, and their fluorescence was measured over time. (a) Raw data showing the average particle signal multiplied by the number of particles vs incubation time. (b, left) Dimensionless signal vs dimensionless time showing the collapse of the data from panel a onto a universal curve. The dashed line represents a fit of eq 20 to the data with $k_d D_{gel} = 5.5 \times 10^{-5}$ m$^2$ s$^{-2}$ M$^{-1}$ and $F_{e,FITC} = 2.54 \times 10^{12}$. (b, right) The observed fluorescence plotted against the model fit. The dashed line ($x = y$) represents a perfect fit and is shown to guide the eye.



mechanics), a probe concentration of 50 $\mu$M in precursor solution (for 5.5 $\mu$M in particles after 11% incorporation efficiency), and thin, 30 $\mu$m probe regions. We investigated hybridization times up to 3.3 h, at which point the reaction is expected to be ~75% complete (i.e., $\tau \sim 1.3$ so $\tilde{T}_s = 0.25$ using eq 18). It is important to note that this is much shorter than typical assay times for commercially available multiplexing systems, which frequently recommend incubations up to 20 h or more.[36,37]

For sensitivity assays, we chose to use phycoerythrin (i.e., SAPE) as the reporting fluorophore, as it is much more efficient than fluorescein used in our model validation, but requires an extra processing step to report fluorescence. In a typical assay, particles are incubated with biotinylated targets and subsequently labeled using SAPE in a 30 min reaction. We found the fluorescent efficiency for SAPE assays, using our detection system, to be $F_{e,SAPE} = 2.5 \times 10^{14}$ AU m$^2$/mol.

To measure the detection limits experimentally, we incubated particles with target at varying levels near the expected limits. For each concentration, the fluorescent signal was measured and divided by the pooled standard deviation of the background signal (over all measurements) to obtain a signal-to-noise ratio (S/N). A line was then fit to the S/N data for each time point, specifically for the three data points above the limit of detection (LOD) (data not shown), to obtain and estimate of the sensitivity, which we designated as the point where S/N = 3. With the use of our detection settings, the observed noise is typically ~0.5 AU, such that at the LOD the signal, $I$, would be ~1.5 AU.

As shown in Figure 4, our system is extremely sensitive, providing subattomole LODs even with short, 1 h hybridizations. Furthermore, the dynamic nature of this sensitivity is predictable using our model, as indicated by in the figure. The sensitivity and kinetics of our system are very favorable compared to commercially available systems and will likely improve with the implementation of photomultiplier-based detection.

**Investigation of Specificity.** We demonstrated the optimization of particle design for highly sensitive detection. Another important metric for nucleic acid detection is specificity—how well the assay can distinguish between closely related targets. In order to show that the optimized particle design and labeling scheme do not negatively affect the specificity of our system, we investigated the cross-reactivity of an RNA target with a closely related

(36) Castoldi, M.; Schmidt, S.; Benes, V.; Noerholm, M.; Kulozik, A. E.; Hentze, M. W.; Muckenthaler, M. U. *RNA* **2006**, *12*, 913–920.
(37) Wang, H.; Ach, R. A.; Curry, B. *RNA* **2007**, *13*, 151–159.

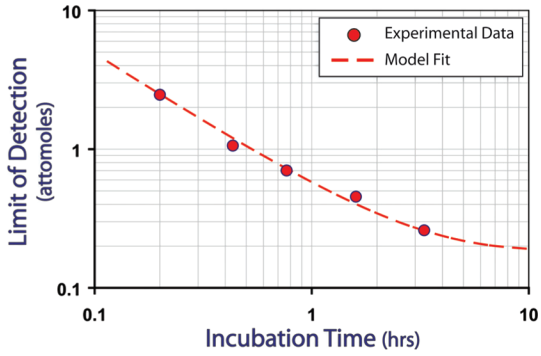


**Figure 4.** Assessment of assay sensitivity vs model predictions. Particles were incubated with varying amounts of target, and signal-to-noise ratios were calculated. The sensitivity was taken at the target concentration where S/N = 3. The model fit comes from a rearrangement of eq 19 with $I = 3 \times$ noise, such that $V_s[T_s]_o = 1.5N_pA_p/(F_{e,SAPE}(1 - e^{-r}))$.

complementary probes. As a model system, we chose to investigate the microRNA let-7 family, as has been done extensively in the literature.[37−39]

We synthesized particles bearing four unique regions, containing four probes for let-7 family members (7a−7d), which vary by only one or two nucleotides in sequence. The probes were incorporated at a precursor concentration of 10 $\mu$M (or ~1.1 $\mu$M in the particles). Particles were incubated with samples containing 5 fmol of biotinylated let-7a RNA and 500 ng of total *E. coli* RNA to add complexity, thus mimicking a "real" assay that would likely involve total human RNA consisting of broadly heterogeneous nucleic acid mixtures. Incubations were 1 h at 58 °C with 0.5 M NaCl in the hybridization buffer.

Our results (Figure 5) show that we can achieve single-nucleotide specificity with less than 3% cross-reactivity. This indicates that the particle composition and labeling scheme we use are suitable for both highly sensitive and highly specific nucleic acid quantification. As mentioned previously, other technologies rely on sophisticated probe design[37] or modification[36] to show single-nucleotide specificity. Due to the nonfouling nature and solution-like thermodynamics of our hydrogel substrates, we were able to achieve this without need of these devices.

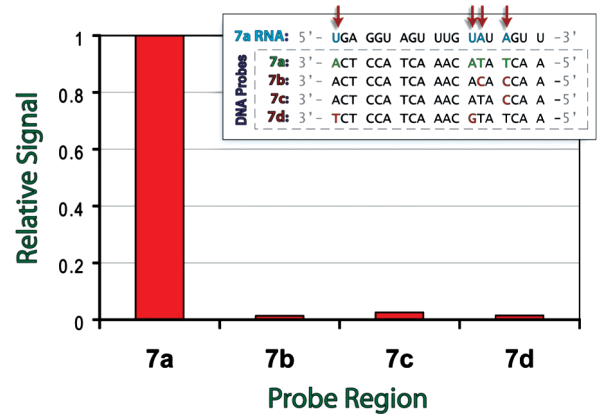


**Figure 5.** Assessment of assay specificity across closely related probes. An RNA target was incubated with particle bearing four probes, one completely complementary and three varying by one or two nucleotides. Shown is the relative signal for target capture in each probe region.

## CONCLUSIONS

We have optimized hydrogel particle composition and design for highly sensitive nucleic acid quantification. We have developed and validated a quantitative model that provides insight into the parameters dictating assay kinetics and sensitivity. Using an optimized particle design and an efficient fluorescent labeling scheme, we showed subattomole sensitivity with short incubations of an hour. Lastly, we demonstrated that, using these particles, we could achieve single-attomole specificity with very little cross-reactivity. The excellent sensitivity, specificity, and kinetics of our system are dictated by the solution-like thermodynamics of hybridization in hydrogel substrates and particle-based nature of our assays. The high-performance detection demonstrated here, along with the high-density coding ability, rapid flow-through scanning, and low cost previously demonstrated[25] makes our system ideal for discovery and clinical diagnostics.

## ACKNOWLEDGMENT

We gratefully acknowledge support from MIT's Deshpande Center, the MIT CSBi Merck Fellowship, and Grant R21EB008814 from the National Institute of Biomedical Imaging and Bioengineering, National Institutes of Health. We also thank Anthony Balducci, Stephen Chapin, and Daniel Trahan for useful discussion.

Received for review March 12, 2009. Accepted April 19, 2009.

AC9005292

(38) Lu, J.; Getz, G.; Miska, E. A.; Alvarez-Saavedra, E.; Lamb, J.; Peck, D.; Sweet-Cordero, A.; Ebet, B. L.; Mak, R. H.; Ferrando, A. A.; Downing, J. R.; Jacks, T.; Horvitz, H. R.; Golub, T. R. *Nature* **2005**, *435*, 834–838.

(39) Chen, C.; Ridzon, D. A.; Broomer, A. J.; Zhou, Z.; Lee, D. H.; Nguyen, J. T.; Barbisin, M.; Xu, N. L.; Mahuvakar, V. R.; Andersen, M. R.; Lao, K. Q.; Livak, K. J.; Guegler, K. J. *Nucleic Acids Res.* **2005**, *33*, e179.